Classification of Parotid Gland Tumors using Sonohistology

Stefan Siebers[1,4], Ulrich Scheipers[1,4], Frank Gottwald[2], Alessandro Bozzato[2], Martin Mienkina[3,4], Johannes Zenk[2], Heinrich Iro[2] and Helmut Ermert[1,4]

[1]Institute of High Frequency Engineering, Ruhr-University, Bochum, Germany
[2]University Hospital for Otorhinolaryngology, Friedrich-Alexander University Erlangen-Nuremberg, Germany
[3]Institute of Medical Engineering, Ruhr-University, Bochum, Germany
[4]Ruhr Center of Excellence for Medical Engineering (KMR), Bochum, Germany

stefan.siebers@rub.de

***Abstract* – In this paper results from a clinical study on differentiating between various types of parotid gland tumors using computerized tissue characterization (Sonohistology) are presented. Complex baseband ultrasound data have been acquired during the common examinations of patients who were scheduled to have parotid surgery shortly after the acquisition. Data of 123 benign and malignant parotid-gland alterations have been included in the study. For data acquisition, a conventional diagnostic ultrasound scanner controlled by custom software running on a laptop computer was used. Tumors were manually contoured in the B-Mode images. Acquired data were stored on an external PC and subdivided into numerous regions of interest (ROI). For each ROI, a set of tissue characterizing spectral and texture features was calculated. Moreover, Fourier descriptors have been calculated from the contours of the lesions to characterize differences in shape of certain kinds of tumors. Training data have been generated from the manually contoured areas. For classification, the training data have been divided in up to four subclasses. The final classification was done using two target classes. The first class included all cases for which a surgical treatment was definitely necessary. The second class included all cases that did not necessitate a surgical treatment. The best feature set was processed by a classification system. For classification, the maximum likelihood measure was used. Classification was done by total cross validation over cases. The best feature set was found by sequential forward selection and included two spectral features (attenuation and slope), two first order texture feature (squared signal to noise ratio and kurtosis), two measures from the cooccurrence matrix (sum variance and variance of sum of squares) and two Fourier descriptors. The receiver operating characteristics curve area was $A_{\mathrm{ROC}} = 0.86$.**

Keywords - tissue characterization; classification; texture features; spectral features; parotid gland; cancer diagnostics; ultrasound; sonography;

I. INTRODUCTION

The parotid glands are the largest of the salivary glands in the head and neck region. They are located between the outer ear and the lower jaw, embedded in the subcutaneous tissue of the face. Usually parotid gland tumors are removed surgically by partial or complete gland excision. However, although new surgical techniques including nerve monitoring are described, the intraglandular course of the facial nerve makes parotid surgery a challenging intervention.

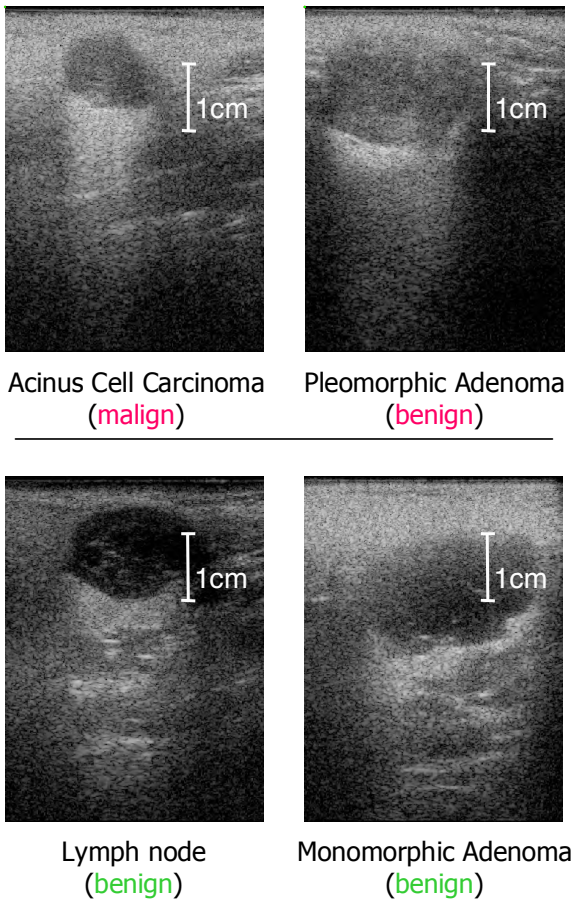

Figure 1. Exemplary B-mode images. Top: two positive cases (acinus cell carcinoma and pleomorphic adenoma, which actually is benign, but should be treated). Bottom: two negative cases (lymph node and monomorphic adenoma, both could be left untreated).

In otorhinolaryngology, the incidence of parotid gland tumors is one of the highest of all incidences of tumors. Commonly, differentiation between benign and malignant lesions is difficult. In addition, some types of benign parotid gland tumors, such as pleomorphic adenomas, may become malignant at later stages of the disease. Since not all kinds of tumors or alterations must undergo medical treatment, exact diagnostic modalities are desired to avoid unnecessary surgeries. The goal of this work is to differentiate between cases where surgical treatment is inevitable, and those which must not necessarily be treated.

In general, B-mode imaging is applied as the main diagnostic modality in order to differentiate among the various types of parotid gland tumors. Four typical examples of tumors and alterations of the parotid gland are shown in Figure 1.

Although the tumor or alteration of the parotid gland can be easily located using diagnostic imaging, modalities including medical ultrasound and MRI are reported to be too inexact when it comes to differentiate between benign and malignant forms of alterations [1]. Currently, only the histopathologic examination of tissue specimen can provide the information needed for a definitive diagnosis. Biopsies are considered to be questionable by many physicians, since they have a certain rate of misclassification and, in addition, the facial nerve may also be affected.

In this paper, it is shown, that the application of Sonohistology (ultrasonic tissue characterization) can add additional information to the currently available methods of diagnostics.

In the past, automated tissue characterization using several features extracted from backscattered ultrasound signals has been used in many research projects. In particular, tissue characterization was applied to differentiate between various kinds of biological tissue, e.g. in prostate diagnostics [2,3] or for monitoring of thermal therapies [4]. For the characterization of parotid-gland tumors, preliminary results from the same study presented in this paper showed promising results [5,6].

II. Materials and Methods

A. Clinical Study and Data Acquisition

Baseband ultrasound echo data of the parotid gland were captured during the routine examination of the patient using standard ultrasound imaging equipment. Patient compliance to the procedure was high, as the new method does not extend the normal examination time when applying ultrasound imaging to the head and neck region.

For the clinical study, a Siemens Elegra digital ultrasound scanner equipped with a research interface was used. The linear probe (7.5L40) was set to a center frequency of 7.2 MHz. For every frame, 2400 samples were recorded for 360 lines. The approximate size of the images was 5.1 cm in axial direction and 4 cm in lateral direction, respectively. The single transmit focus was set to a depth of 2 cm. Radio frequency echo data were acquired at 36 MHz and 12 bits.

Controlling of the Elegra was done using custom made software (SynchroSuite, KMR, Bochum, Germany) running on a laptop computer. Baseband data was acquired by accessing the internal operation system of the Elegra via telnet and downloading the data via FTP. A dump file containing all relevant parameters of the Elegra was also stored along with each frame and used later to compensate for TGC settings. Two orthogonal frames per lesion were recorded.

The tumors were manually contoured in the B-mode images by an experienced physician to define an area of interest. Thus, it was ensured that only signals originating from the tumors and not from surrounding tissue have been used for feature extraction and classification.

During the routine examination, the diagnosis of an experienced physician on the basis of ultrasound B-mode imaging, occasional Doppler imaging, palpation and anamnesis was recorded. Histopathological examinations after parotidectomy were used as the "gold standard". The results of histologic examinations and subdivision into different classes (see section C) are shown in Table 1.

TABLE I. Occurrence of different types of parotid gland tumors and alterations during the clinical study and subdivision into subclasses and target classes

Type of tumor	***n***	subclass	target class
Pleomorphic adenoma	28	Ω_{Spos1}	Ω_{pos}
Acinus cell carcinoma	6	Ω_{Spos2}	
Other Carcinomas	6		
Lymphoma	4		
Metastasis	4		
Monomorphic adenoma	38	Ω_{Sneg1}	Ω_{neg}
Basal cell adenoma	11	Ω_{Sneg2}	
Lipoma	3		
Lymph nodes	8		
Nodular fasciitis	1		
Cyst	12		
Canaliculous adenoma	1		
Adenoid cyst	1		

B. Feature Extraction

During the common B-mode examination, the physician tries to classify a tumor, among other things, according to its texture, echogenicity, and shape. Hence, for the automated classification, tissue characterizing features from spatial and spectral domain were used in this study to account for differences in texture and echogenicity, respectively. In addition, Fourier descriptors were estimated from the manually delineated tumor boundaries to account for differences in shape.

For calculation of textural and spectral features, each data frame was subdivided into numerous regions of interest (ROI). Each ROI is spanned over an area of about 4.6 mm^2 extending approximately 2.7 mm in the axial direction and 1.7 mm in the lateral direction. Thus, the smallest region that can be analyzed by the system covers approximately 4.6 mm^2. The ROIs consist

of 128 sample points in the axial direction and of 16 scan lines in the lateral direction. The axial and lateral overlaps of the ROIs were 50 % each.

ROIs were transformed into frequency domain using Fourier transform on every scan line of the ROI. Before applying the Fourier transform, all ROIs were windowed by a Hamming window of the ROIs length to avoid spectral leakage. The baseband data were compensated for system and depth-dependent effects using the system transfer function over depth as an inverse filter within the effective bandwidth. Using this approach, system effects due to focusing and electro-mechanical characteristics of the transducer can partially be compensated [7, 8].

Estimates of the frequency dependent attenuation coefficient were obtained using the spectral shift method [9]. Midband, slope and intercept values of a straight-line fit to the spectrum served as measures for backscatter [3].

All textural features were calculated after demodulating the RF signals using Hilbert transform. Moreover, for the calculation of second order texture features, image data were quantized to 64 intensity levels. Texture features used in this study included histogram based features as well as features calculated from normalized cooccurrence matrices as proposed by Haralick [10], features from gray level run length matrices [11], and texture energy measures as proposed by Laws [12].

Fourier descriptors [13] were calculated from the manually delineated contour lines. An inner boundary tracing algorithm was used to yield a uniformly sampled representation of the contour in 4-neighborhood (Fig. 2). Fourier descriptors were obtained after discrete Fourier transforming the contour line.

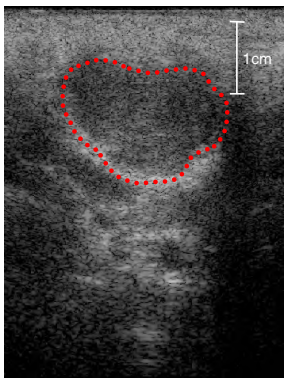

Figure 2. Manually countoured tumor. Dotted line: contour line in 4-neighborhood used for calculation of Fourier descriptors.

C. *Feature Selection and Classification*

Since the goal of this work was to distinguish between cases that must undergo surgical treatment (positive cases) from cases that can be left untreated (negative cases), the tumor types having occurred during this study were subdivided into two target classes, Ω_{pos} and Ω_{neg}. Target class Ω_{pos} comprised all positive cases, i.e. pleomorphic adenomas and all malign alterations, whereas target class Ω_{neg} comprised all negative cases, i.e. monomorphic adenomas and the remaining benign alterations. However, it is evident that mixing too many different cases in one class might not be beneficial, since training data become quite inhomogeneous. Therefore, yet another, finer subdivision of cases was carried out. A total number of four subclasses turned out to be most advantageous. Such, subdivision was done by defining one class each for the two largest groups, pleomorphic and monomorphic adenomas, respectively. These subclasses were Ω_{Spos1} and Ω_{Sneg1}. All malignant cases formed subclass Ω_{Spos2}, whereas all remaining benign cases formed subclass Ω_{Sneg2} (Table 1).

For classification, the maximum likelihood measure was used. Each ROI was classified separately. Classification was performed by leave-one-out validation over cases. Therefore, for classification of one ROI, the remaining ROIs of the same case were left out of the training dataset. In an intermediate step, each feature vector representing an ROI was assigned to the subclass with the maximal likelihood. To obtain binary output maps, the feature vector was then assigned to either target class Ω_{pos} or Ω_{neg}, according to its particular subclass. Averaging of the binary output maps gave a mean decision criterion for each case. The decision criterion could be scaled using an arbitrary threshold. The area under the receiver operating characteristics curve A_{ROC} was used as a quality measure of the classification.

To evaluate each feature separately, a first classification pass was done using one feature at a time. A_{ROC} was determined for each case and used as a performance criterion for each feature. The features were then arranged according to their performance. To find the best performing set of features, a second classification pass started with the active set consisting of the best feature exclusively. After each classification pass the active set was updated with the next feature in the queue. If A_{ROC} increased, the new feature remained in the set, otherwise it was removed again.

III. RESULTS

The current work comprises 123 cases from an ongoing clinical study. The diagnosis of an experienced physician on the basis of common diagnostic modalities during the routine examinations yielded a sensitivity of 0.9 and a specificity of 0.59. Apparently, common diagnosis is uncertain, resulting in a large quantity of dispensable surgeries.

Generation of training data for the Sonohistology approach presented in this paper yielded 16697 ROIs of class Ω_{Spos1}, 9780 ROIs of class Ω_{Spos2}, 19385 ROIs of class Ω_{Sneg1} and 11212 ROIs of class Ω_{Sneg2}. The feature selection algorithm yielded 8 features as the best set of features, including two spectral features (attenuation and slope), two first order texture features (squared signal to noise ratio and kurtosis), two measures from the cooccurrence matrix (sum variance and variance of sum of squares) and two Fourier descriptors. The area under the ROC curve was $A_{ROC} = 0.86$. At the sensitivity of 0.9 reached by the physicians, the classification achieved a

specificity of 0.71. At the specificity of 0.59 reached by the physicians, the classification achieved a sensitivity of 0.94 (Fig. 3).

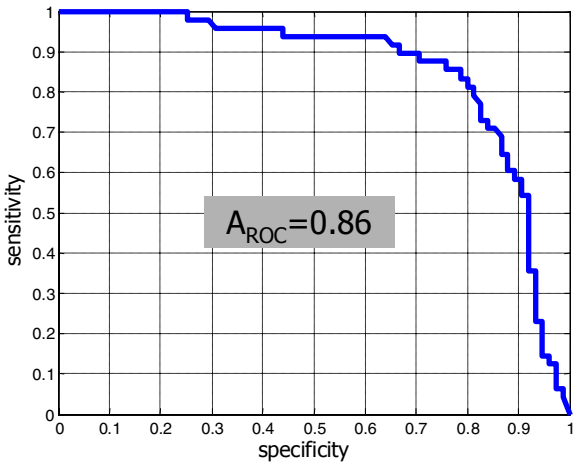

Figure 3. ROC curve of final classification result. The area under the ROC curve is $A_{ROC} = 0.86$. At the sensitivity of 0.9, specificity is 0.71. At a specificity is 0.59, sensitivity is 0.94.

If the system is scaled to reach a sensitivity of 1, which means that all cases that are in need of surgical treatment are detected, the remaining specificity is 0.25.

When using only two subclasses instead of four, the classification rate drops significantly. The area under the ROC curve yields $A_{ROC} = 0.81$ in that case. At a sensitivity of 0.9, specificity is 0.55. At a specificity is 0.59, sensitivity is 0.83.

IV. Discussion and Conclusions

In this paper, a Sonohistology system for the differentiation of various kinds of parotid gland tumors and alterations has been presented. Overall 123 cases from an ongoing clinical study were considered so far. The Sonohistology system for ultrasonic multi feature tissue characterization differentiates between positive cases that must undergo surgical treatment and negative cases that can be left untreated with a satisfying grade of accuracy. The area under the ROC curve is $A_{ROC} = 0.86$ when using four subclasses during classification. Using Sonohistology, negative cases can be detected while still achieving a sensitivity of 1. Therefore, the system can be used to prevent unneeded surgical treatment. This is of importance, since the parotid gland encloses the facial nerve. Thus, parotid gland surgeries can be hazardous.

The classification rates will possibly increase if a larger database is available. Several alterations of parotid glands only occurred once during this study, others only a few times. However, for an appropriate training of the system, a larger number of each incidence is desirable. If so, more subclasses or rather different compositions of subclasses may be beneficial.

Acknowledgements

This work is an activity of the Ruhr Center of Excellence for Medical Engineering (Kompetenzzentrum Medizintechnik Ruhr, KMR) Bochum. It is supported by the German Federal Ministry of Education and Research (Bundesministerium für Bildung und Forschung), grant No. 13N8079.

Ulrich Scheipers is now with Resonant Medical Inc., Montreal, Quebec, Canada.

References

[1] Izzo L, Sassayannis PG et al. The role of Echo Colour/Power Doppler and magnetic resonance in expansive parotid lesions. J Exp Clin Cancer Res. 2004;23(4):585-92.

[2] U. Scheipers, H. Ermert, H.-J. Sommerfeld, M. Garcia-Schürmann, T. Senge, S. Philippou, "Ultrasonic multifeature tissue characterization for prostate diagnostics", *Ultrasound in Medicine and Biology*, Vol. 29, No. 8, pp. 1137-1149, 2003

[3] E.J. Feleppa, C.R. Porter, J.A.Ketterling, P. Lee, S. Dasgupta, S., S. Urban, A. Kalisz, "Recent Developments in Tissue-type Imaging (TTI) for Planning and Monitoring Treatment of Prostate Cancer", *Ultrason. Imaging*, Vol. 26, pp. 163-172, 2004.

[4] S. Siebers, U. Scheipers, M. Ashfaq, J. Hänsler, M. Frieser, D. Strobel, E. Hahn, H. Ermert," In Vivo Imaging of Coagulated Tissue", Proc. IEEE Ultrasonics Symposium 2006, in press

[5] U. Scheipers, S. Siebers, F. Gottwald, M. Ashfaq, A. Bozzato, J. Zenk, H. Iro, H. Ermert, "Sonohistology for the Computerized Differentiation of Parotid-Gland Tumors", *Ultrasound Med Biol,* Vol. 31, No. 10, pp. 1287-1296, *2005*

[6] U. Scheipers, S. Siebers, F. Gottwald, M. Ashfaq, A. Bozzato, J. Zenk, H. Iro, H. Ermert, "Ultrasonic Tissue Characterization for the Differentiation of Parotid Gland Tumors", Proc. IEEE Ultrasonics Symposium 2005, pp.827-830, 2005

[7] Thijssen JM. Spectroscopy and Image Texture Analysis. Ultrasound Med Biol 2000;26:41-44.

[8] Huisman HJ, Thijssen JM. Precision and Accuracy of Acousto-spectrographic Parameters. Ultrasound Med Biol 1996;22:855-871.

[9] M. Fink, F. Hottier, J.F. Cardoso, "Ultrasonic signal processing for in vivo attenuation measurement – short time fourier analysis", *Ultrasonic Imaging*, Vol. 5, pp. 117-135

[10] R.M. Haralick, K. Shanmugam, I. Dinstein, "Textural Features For Image Classification", *IEEE Trans. on Systems, Man, And Cybernetics,* Vol. SMC-3, No. 6, 1973

[11] M. Galloway, "Texture analysis using gray level run lengths", *Computer Graphics and Image Processing,* Vol. 4, pp. 172-179, 1975

[12] K. Laws, "Rapid texture identification", *SPIE Image Processing for Missile Guidance,* Vol. 238, pp. 376-380, 1980

[13] G.H. Granlund, "Fourier Preprocessing for Hand Print Character Recognition", *IEEE Trans. on Computers,* C-21, pp. 195-201, 1972